Int. J. Solids Structures Vol. 14, pp. 851–860

0020-7683/78/1001-0851/$02.00/0

EFFECT OF ACCELEROMETER MASS ON THE FLEXURAL MOTION OF PLATES

NAGYOUNG CHANG,† DAVID P. BILLINGTON‡ and DENNIS A. NAGY§
Department of Civil Engineering, Princeton University, Princeton, NJ 08540, U.S.A.

(*Received* 26 *September* 1977; *in revised form* 13 *February* 1978; *received for publication* 13 *March* 1978)

Abstract—When the flexural acceleration of a plate is measured by an accelerometer, the mass of the accelerometer tends to reduce the magnitude of the acceleration.

This study establishes a simple analytical relation between the accelerometer mass and the corresponding reduction of acceleration. This has been done by studying an idealized diffraction problem for the plate flexural waves.

The complex frequency response depends upon the accelerometer mass, the frequency of the flexural wave, the plate thickness and the material parameters of the plate.

A numerical filtering method is used to bring an experimental result and a corresponding numerical prediction closer together.

INTRODUCTION

It has been observed for some time that, when the flexural acceleration of a plate is measured by an accelerometer, the mass of the accelerometer tends to reduce the magnitude of the acceleration[1]. An experimental study on some precipitator plates indicates that the increase in the accelerometer mass can reduce the magnitude of the measured acceleration by more than 50%[2]. The purpose of this report is to establish a simple analytical relation between the accelerometer mass and the corresponding reduction of acceleration. This has been done by studying an idealized diffraction problem for the plate flexural waves.

Several assumptions have been introduced toward the idealized problem as depicted in Fig. 1. First, the accelerometer is assumed to be a rigid circular cylinder with its center of mass sitting on the neutral plane of the plate. As indicated in Fig. 1, the axis of the cylinder is perpendicular to the plane of the plate. Second, the flexural acceleration of the plate is studied at the center of mass of the cylinder. Third, the flexural motion of the plate is governed by the classical flexural theory of the plate. Fourth, the plate is infinite and has no boundary. Fifth, a one-dimensional, propogating wave is incident upon the cylinder, where it is diffracted.

REDUCTION FACTOR

Consider the plate-accelerometer model of Fig. 1. The plate is infinite, and a homogeneous, rigid circular cylinder is rigidly attached to the plate. Both the cartesian coordinates x, y and the polar coordinates r, θ are used in this report, and the origin of these coordinates coincides with the center of mass of the cylinder. The flexural vibration of the plate is governed by the classical flexural theory of plates[3], hence the equation of motion:

$$[Eh^3/12(1-\nu^2)]\nabla^2\nabla^2 u + \rho h\ddot{u} = 0, \tag{1}$$

and the constitutive equations:

$$\begin{aligned} q_r &= -[Eh^3/12(1-\nu^2)]\nabla^2 u_{,r} \\ m_r &= -[Eh^3/12(1-\nu^2)][u_{,rr} + \nu r^{-2}u_{,\theta\theta} + \nu r^{-1}u_{,r}], \\ m_{r\theta} &= -[Eh^3/12(1+\nu)][r^{-1}u_{,r\theta} - r^{-2}u_{,\theta}], \end{aligned} \tag{2}$$

†Research Associate.
‡Professor of Civil Engineering.
§Assistant Professor.

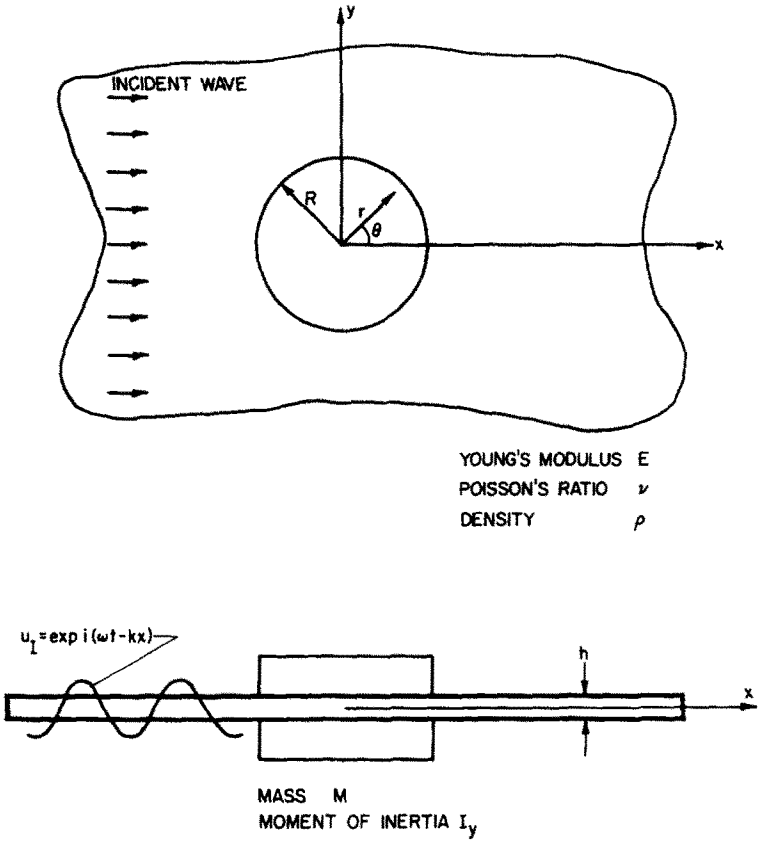

Fig. 1. Plate-accelerometer model.

where E, ν, ρ and h are the Young's modulus, Poisson's ratio, density and the thickness of the plate respectively, u, q_r, M_r and $M_{r\theta}$ are the flexural displacement, shear force per unit length, bending moment per unit length, and the twisting moment per unit length on a plate cross section whose outward normal vector is in the positive direction. Also,

$$[\ ]_{,r} \equiv \partial[\ ]/\partial r, \quad [\ ]_{,\theta} \equiv \partial[\ ]/\partial\theta, \quad [\dot{}] \equiv \partial[\ ]/\partial t,$$

where t represents the time, and ∇^2 is a Laplacian operator. The rigid circular cylinder (accelerometer) is described by three parameters, the radius R, its mass M, and the second moment of inertia around the y-axis, I_y.

At a given frequency ω, a one-dimensional, propagating wave u_I is incident upon the cylinder:

$$u_I = \exp i(\omega t - kx) = \exp i(\omega t - kr\cos\theta), \quad r \geq R \tag{3}$$

A diffracted wave, u_D, is generated due to the presence of the cylinder, and so the total displacement field in the plate:

$$u = u_I + u_D, \quad r \geq R \tag{4}$$

Since the incident wave is a solution of (1), there is a unique relation between the frequency ω and the (positive) wave number k, i.e.

$$[Eh^3/12(1-\nu^2)\rho]k^4 = \omega^2, \tag{5}$$

which determines k from ω. The diffracted wave u_D is a periodic function of θ with a period 2π. Because of the symmetry of the problem with respect to the x-axis, u_D is also an even function

of θ. Hence, the diffracted wave u_D may be expanded in $\cos n\theta$, $n = 0, 1, 2, \ldots$:

$$u_D = [F_0(r) + \sum_{n=1}^{\infty} F_n(r) \cos n\theta] \exp(i\omega t), \tag{6}$$

where $F_0, F_1, F_2 \ldots$ are to be determined from the condition that each term in the above series be a solution to (1). From this condition and (5) we get a series of differential equations:

$$(D^2 + r^{-1}D - n^2r^{-2} + k^2)(D^2 + r^{-1}D - n^2r^{-2} - k^2)F_n = 0,$$
$$n = 0, 1, 2, \ldots, \tag{7}$$

where $D[\ ] = d[\ ]/dr$. Hence, the general solution [3]:

$$F_n = a_{n1}H_n^{(2)}(kr) + a_{n2}K_n(kr) + a_{n3}H_n^{(1)}(kr) + a_{n4}I_n(kr),$$
$$n = 0, 1, 2, \ldots, \tag{8}$$

where $H_n^{(1)}$ and $H_n^{(2)}$, are Hankel functions of the first and second kind and I_n and K_n are modified Bessel functions of the first and second kind. For each order n the diffracted wave consists of two terms: one that represents the outward traveling, and the other that decays outward [4]. Therefore, the general solution of the diffracted wave becomes

$$u_D = \left[a_{01}H_0^{(2)}(kr) + a_{02}K_0(kr) + \sum_{n=1}^{\infty} \{a_{n1}H_n^{(2)}(kr) + a_{n2}K_n(kr)\} \cos n\theta\right] \exp(i\omega t). \tag{9}$$

It is also possible to expand the incident wave (3) in $\cos n\theta$, $n = 0, 1, 2, \ldots$ [4]:

$$u = \left[J_0(kr) + \sum_{n=1}^{\infty} 2(-i)^n J_n(kr) \cos n\theta\right] \exp(i\omega t), \tag{10}$$

where $J_0, J_1, J_2, \ldots$ are the Bessel functions of the first kind. Substituting (9) and (10) into (4),

$$u = [J_0(kr) + a_{01}H_0^{(2)}(kr) + a_{02}K_0(kr)$$
$$+ \sum_{n=1}^{\infty} \{2(-i)^n J_n(kr) + a_{n1}H_n^{(2)}(kr) + a_{n2}K_n(kr)\} \cos n\theta\Big] \exp(i\omega t),$$
$$r \geq R. \tag{11}$$

There are two undetermined constants at each order n, i.e. a_{n1} and a_{n2}. They are to be determined from boundary conditions around the circumference of the cylinder.

Due to the symmetry of the problem with respect to x-axis, the rigid circular cylinder can have only two degrees of freedom, namely the translation in the direction normal to the plane of the plate, and the rotation around the y-axis. Thus for small motion, the displacement v of the cylinder can be represented by

$$v = [G + Ar \cos\theta] \exp(i\omega t), \quad r \leq R, \tag{12}$$

where G is the (complex) amplitude of the translatory motion of the center of mass of the cylinder, and A is the (complex) amplitude of the angle of rotation of the cylinder around y-axis. In the absence of the cylinder the incident wave u_i of (3) would be the only solution for the entire plate, and the amplitude of the flexural motion at the origin would be unity. The presence of the cylinder modifies the solution such that the amplitude of the flexural motion at the origin be G, and so G represents the complex frequency response [5]. The quantity $|G|$ then represents a frequency dependent reduction factor in the sense that, to calculate the magnitude of the acceleration measured by an accelerometer, one has to multiply the acceleration which would occur in the absence of the accelerometer by $|G|$.

Two equations of motion must be satisfied by the rigid circular cylinder. For the translatory

motion:

$$\int_{-\pi}^{\pi} [q_r]_{r=R} R \, d\theta = -MG\omega^2 \exp(i\omega t), \tag{13}$$

and for the rotatory motion:

$$\int_{-\pi}^{\pi} [q_r r \cos\theta - m_r \cos\theta + m_{r\theta} \sin\theta]_{r=R} R \, d\theta = -1_y A\omega^2 \exp(i\omega t). \tag{14}$$

Since the cylinder is rigidly connected to the plate, the displacement and the radial gradient of the displacement must be continuous around the circumference of the cylinder:

$$[u]_{r=R} = [G + AR\cos\theta] \exp(i\omega t), \quad -\pi \le \theta \le \pi, \tag{15}$$

$$[Du]_{r=R} = [A\cos\theta] \exp(i\omega t), \quad -\pi \le \theta \le \pi. \tag{16}$$

Equations (13)–(16) offer just enough number of conditions for determining $G, A, a_{01}, a_{02}, a_{11}, a_{12}, \ldots$ In this report we are interested in G only, the complex frequency response of the accelerometer.

To solve for G, we choose the following three equations out of all those implied by (13)–(16):

$$\begin{aligned} -2\pi R[Eh^3/12(1-\nu^2)][(D^2 + r^{-1}D)D\{J_0(kr) + a_{01}H_0^{(2)}(kr) + a_{01}K_0(kr)\}]_{r=R} &= M\omega^2 G, \\ J_0(kR) + a_{01}H_0^{(2)}(kR) + a_{02}K_0(kR) &= G, \\ [D\{J_0(kr) + a_{01}H_0^{(2)}(kr) + a_{02}K_0(kr)\}]_{r=R} &= 0. \end{aligned} \tag{17}$$

The first of (17) is obtained by substituting (11) into q_r of (2) and using the result in (13). The second of (17) follows from the integration of (15) fro $\theta = -\pi$ to $\theta = \pi$. The third of (17) comes from the integration of (16) from $\theta = -\pi$ to $\theta = \pi$. Three undetermined constants, G, a_{01}, and a_{02}, are coupled in (17). We now recall the following identities [6]:

$$\begin{aligned} (D^2 + r^{-1}D - n^2r^{-2} + k^2)\Phi_n(kr) &= 0, \quad \text{for } \Phi = J, H^{(2)}, \\ (D^2 + r^{-1}D - n^2r^{-2} - k^2)\Phi_n(kr) &= 0, \quad \text{for } \Phi = K, \\ D[r^{-n}\Phi_n(kr)] &= -kr^{-n}\Phi_{n+1}(kr), \quad \text{for } \Phi = J, H^{(2)}, K. \end{aligned} \tag{18}$$

Using these identities in (17) and solving the result for G, we obtain

$$G = [J_0(kR) - J_1(kR)H_0^{(2)}(kR)/H_1^{(2)}(kr)/[1 + (Mk/4\pi\rho Rh)\{K_0(kr)/K_1(kR) - H_0^{(2)}(kR)/H_1^{(2)}(kR)\}], \tag{19}$$

where k is a positive root of (5), given ω.

The diffraction of flexural waves by a circular rigid inclusion in an elastic plate has been studied by Chou (a master's thesis written in Chinese), and some of his results have been discussed by Pao and Mow [7]. His approach is the same as ours, although the results discussed in [7] are concerned only with the dynamic stress concentration factors. His equation for the rotatory motion of the rigid circular cylinder, as appears on p. 340 of [7], is in conflict with our equation (14). It appears that the formulation in [7] is incomplete since it does not contain the twisting moment $m_{r\theta}$ and since the factor r is left out of the term containing q_r in (14). Since we have not made use of (14) to derive (19), our complex frequency response is not affected by this question. In any event, [7] does give some justification for our assumptions that the propagating wave be used as the incident wave.

It is worth noting that the complex frequency response does not depend upon the moment of inertia of the accelerometer. It depends upon the following three non-dimensional

parameters:

$$\Omega = 2\pi[12(1-\nu^2)\rho/E]^{1/2}hf,$$
$$M_0 = M/\rho h^3 \tag{20}$$
$$\rho_0 = M/\pi\rho R^3,$$

where f is the frequency of the wave in Hertz. In this non-dimensionalization scheme, Ω is a non-dimensional frequency, M_0 is a non-dimensional mass, and ρ_0 is a non-dimensional density. For B and K accelerometers, ρ_0 appears to fall in the range $1.0 \sim 5.0$, and in many cases $\rho_0 \approx 2$. Also, the actual evaluation of (19) indicates that, for $1.0 < \rho_0 < 5.0$, the reduction factor $|G|$ is practically insensitive to the change in ρ_0. On this ground, we have set ρ_0 at 2.0. For precipitator plates the parameter range $0 \leq M_0 \leq 4000$, $0 \leq \Omega \leq 0.1$, appears to cover most practical situtations. The reduction factor $|G|$ has been computed from (19) in this parameter range, and the results are plotted in Figs. 2 and 3.

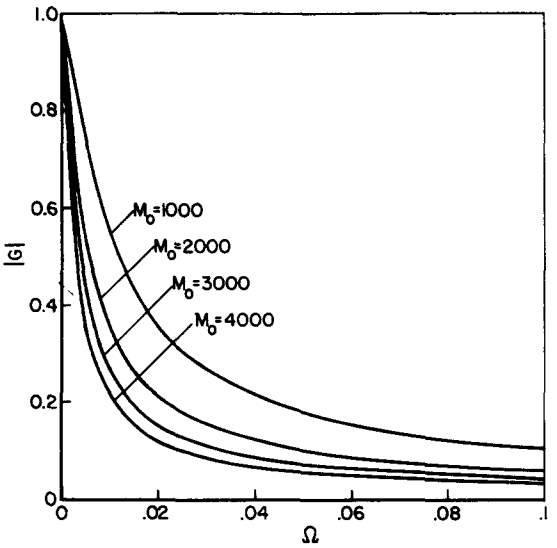

Fig. 2. Reduction factor vs frequency.

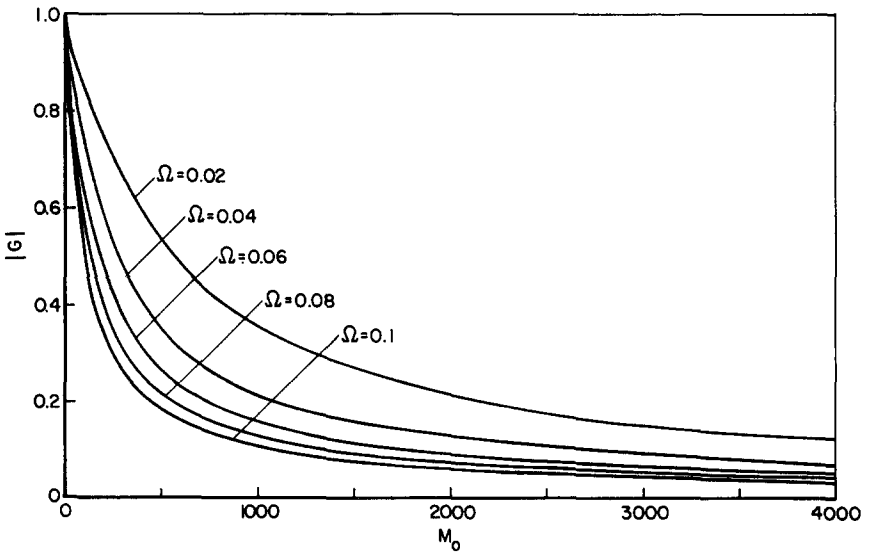

Fig. 3. Reduction factor vs accelerometer mass.

We will illustrate the use of these curves in the following example:

plate thickness	$h = 0.0478$ in. (18 gage plate),
Young's modulus	$E = 3 \times 10^7$ psi,
density	$\rho = 7.2 \times 10^{-4}$ lb sec^2/in^4
Poisson's ratio	$\nu = 0.3$,

dominant frequency of the incident flexural wave $f = 5000$ Hz, accelerometer mass M = 20 g = 1.142×10^{-4} lb sec^2/in. For this example we proceed as follows:

$$\Omega = 2\pi[12(0.91)(7.2 \times 10^{-4})/(3 \times 10^7)]^{1/2}(0.0478)5000 = 0.0243$$
$$M_0 = 1.142 \times 10^{-4}/[(7.2 \times 10^{-4})(0.0478)^3] = 1452$$

Then, both Figs. 2 and 3 give the reduction factor $|G| = 0.26$. This means that acceleration due to a 5 KHz frequency component will get reduced to almost one fourth of its original value by the presence of a 20 g accelerometer on an 18 gage plate. Section 4 below shows how charts can be generated to aid in actual precipitator plate experiments.

Figures 2 and 3 indicate that $|G| \to 0$ as the frequency increases or when the accelerometer mass increases. Also $|G| \to 1$ as the frequency decreases or when the accelerometer mass is reduced. Using the asymptotic equations of Bessel functions[8], we have obtained the following asymptotic forms of (19):

$$\lim_{kR \to \infty} G = [1 + (1 + i)(Mk/4\pi\rho Rh)]^{-1}[2/\pi kR]^{1/2} \exp i(kR - \pi/4),$$
$$\lim_{kR \to 0} G = 1 + 0.5(kR)^2 \ln(kR) - iMk^2/8\rho h. \tag{21}$$

The above asymptotic equations agree with our observations that the reduction factor decreases as the frequency increases, and that the reduction factor becomes unity at zero frequency.

Studies have also been made about the influence of accelerometer mass on measured in-plane accelerations. It has been found[9] that this influence is practically insignificant, being less than 6% for the case of a 20 g accelerometer mounted on an 18 gage plate with an incident plate-extensional wave[10] of 5 KHz frequency.

Miles[11] has computed the complex frequency of the cylinder for a much wider range of k_pR than is considered here. His results also show that $|G_p| \approx 1$ for the range encountered in precipitator plates.

NUMERICAL FILTERING

We now present an application of the complex frequency response G to an actual precipitator plate test. An 18 gage plate, 18 in. wide and 30 ft high, was given a flexural excitation at its top in Research-Cottrell, Inc., Bound Brook, New Jersey[2]. Accelerometers were installed at three stations: the first one at 24.5 in. distance from the top, the second one at 15 ft from the top, and third one at 24.5 in. from the bottom end of the plate. For the first station a numerical result has been obtained[12]. In this numerical work the plate has been assumed to be one-dimensional, and so the local effect of the accelerometer mass was not accounted for. To compare it with the experimental data, it was necessary to process the numerical result. Thus, using this numerical result as an input, we have employed a numerical filtering scheme to apply the complex frequency response G to all the frequency components of the input. Then, the output of this numerical filter should be more comparable to the experimental data.

Let us denote the input numerical data by $p(t)$ and the filtered output by $q(t)$. If we denote the Fourier transform of $p(t)$ and $q(t)$ by $\bar{p}(\omega)$ and $\bar{q}(\omega)$, respectively, then[5]

$$\bar{q}(\omega) = G(\omega)\bar{p}(\omega). \tag{22}$$

Since the input q consists of a finite number of discrete time data, a Fourier series representation may be used. Suppose

$$p(t_l) = \sum_{j=0}^{J} [b_j \cos \omega_j t_l + c_j \sin \omega_j t_l],$$
$$q(t_l) = \sum_{j=0}^{J} [\hat{b}_j \cos \omega_j t_l + \hat{c}_j \sin \omega_j t_l + \hat{c}_j \sin \omega_j t_l], \quad l = 0, 1, 2, \ldots L, \tag{23}$$

where b_j, c_j, $\hat{b}_j$ and $\hat{c}_j$ are the Fourier coefficients, and

$$\omega_j = 2\pi j/(t \max - t \min), \quad j = 0, 1, 2, \ldots J,$$
$$t_l = t \min + (t \max - t \min) l/L, \quad l = 0, 1, 2, \ldots L. \tag{24}$$

In this case (22) becomes

$$\hat{b}_j = Re[G(\omega_j)]b_j + Im[G(\omega_j)]c_j,$$
$$\hat{c}_j = Re[G(\omega_j)]c_j - Im[G(\omega_j)]b_j, \quad j = 0, 1, 2, \ldots J. \tag{25}$$

Then, the numerical filtering can be accomplished as follows:

(1) Using the input time data $p(t_0), p(t_1), p(t_2) \ldots p(t \max)$, compute the Fourier coefficients b_j, c_j, $j = 0, 1, 2, \ldots J$ [see (23)].

(2) Compute the Fourier coefficients $\hat{b}_j$ and $\hat{c}_j$ of the filtered data, using (25).

(3) Construct the filtered data from the second of (23).

Using the above algorithm we have filtered the numerical result[12] for three different values of accelerometer mass, i.e. 6, 35.5 and 83 g. The precipitator plate is an 18 gage steel plate, and so $h = 0.0478$ in., $E = 3 \times 10^7$ psi, $\rho = 7.2 \times 10^{-4}$ lb sec^2/in^4, $\nu = 0.3$. The three sets of filtered data are plotted in Fig. 4 along with the unfiltered data (in dotted line). They have been normalized by the peak acceleration of the unfiltered data, i.e. 139 g (where g is the gravitational acceleration of the earth). The peak value of each set of filtered data is shown in Table 1 along

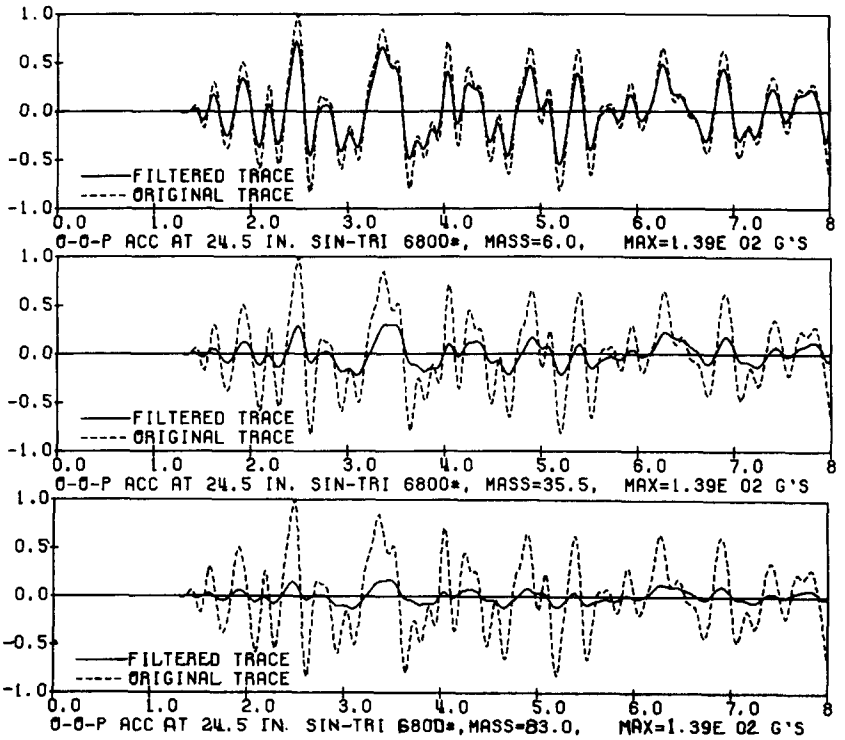

Fig. 4. Accleration time histories, filtered and original.

Table 1. Effect of accelerometer mass on the peak acceleration.

Accelerometer Mass (gram)	Experimental Peak (g)	Numerical Peak (g)
0	·	139
6	130	99
35.5	80	42
83	50	24

with the experimental peak values measured by three different accelerometers[2]. Since it was somewhat difficult to define the "peak value" in the experimental result, we have measured the peak value independently from the experimental data for $t = 0 \sim 8$ m/sec (the time period for which the numerical result is available). Part of the reason why the experimental values are greater than the numerical ones is that the eccentric accelerometer weight caused the in-plane motion to increase the out-of-plane acceleration. This behavior was not included in the numerical study[12]. Even still, the numerical filtering by increasingly greater accelerometer mass appears to bring about the reduction of the peak acceleration by about the same proportion as observed experimentally. Also, the experimental data[2] seem to indicate that the reduction of the peak values is a result of filtering mainly the high frequency components.

ACCELEROMETER MASS INFLUENCE DIAGRAMS

When measuring out-of-plane (flexural) accelerations on experimental or actual precipitator configurations, it is important to have some means of assessing the effect of the accelerometer mass upon the measured results. In practice it would be very useful to select an accelerometer mass such that the measured acceleration is reduced by no more than say, 20% below the acceleration which would actually occur in the absence of the accelerometer. Or, given a particular accelerometer, it would be useful to have an upper bound on the reduction of acceleration.

The reduction factor concept derived in Section 3 of this report can be used to generate charts or diagrams for quickly estimating such effects. Figures 2 and 3, plotted in dimensionless form, can be useful in illustrating the general relationships between mass, frequency, and reduction of acceleration. It is also possible to plot acceleration reduction contours as functions of accelerometer mass and vibration frequency for different gages of steel plating. Three such diagrams, for 16, 18 and 20-gage steel, are shown in Figs. 5, 6 and 7, respectively. Because of the fact that acceleration reduction is an increasing function of frequency, such diagrams can be used to determine upper bounds on acceleration reduction, if some information about the frequency content of the flexural waves is known. It should be remembered that these results are strictly true only for infinitely extending plates and plane flexural waves; however, the size of typical accelerometers is usually very small compared to the distance to the edges or baffles in actual precipitator plates so that it is felt that these results are still very good in such cases.

Two situations of practical interest can utilize such diagrams as Figs. 5, 6 and 7:

(1) Determination of allowable accelerometer mass: if the goal in an experiment or actual field test is to be certain that the measured acceleration is no more than a given percentage below the actual value, the diagrams can be used to determine the maximum allowable accelerometer mass. For example, if the highest significant frequency component is known to be no greater than 3000 Hz and 18-gage steel plates are being measured, then the requirement of no more than 30% acceleration reduction implies, via Fig. 6, that the accelerometer mass should be no greater than 5 g.

(2) Determination of upper bound on acceleration reduction: if certain other considerations dictate the choice of accelerometer, the diagrams may be used to find the upper limit on reduction of the actual acceleration. Using the above example again, a 5 g. accelerometer and knowledge that 3000 Hz is the largest significant frequency shows, on Fig. 6, that the measured acceleration will be no more than 30% below the actual acceleration.

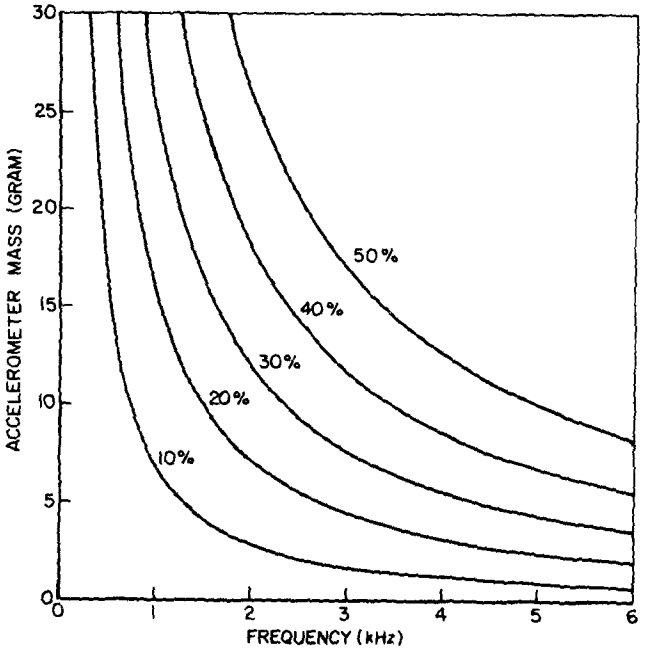

Fig. 5. Acceleration reduction contours 16 gage plate (0.0598 in.).

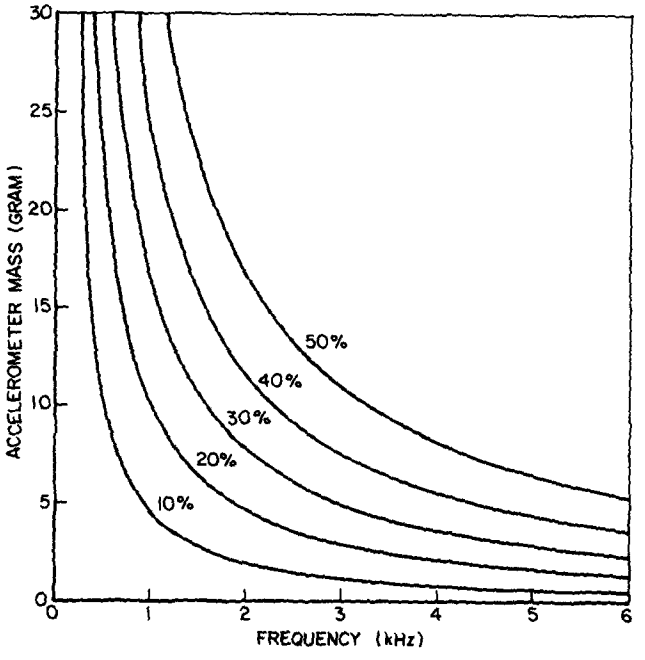

Fig. 6. Acceleration reduction contours 18 gage plate (0.0478 in.).

CONCLUSION

We have studied the effect of accelerometer mass on the flexural accleration of plates using the diffracted wave approach. An analytic expression (19) has been obtained for the complex frequency response. It has been found that the complex frequency response depends upon the accelerometer mass, the frequency of the flexural wave, the plate thickness and the material parameters of the plate. In addition to two non-dimensional charts for computing the reduction factor (Figs. 2 and 3), we have indicated, in Section 4, how the results of this report may be used to generate contours for judging the effect of accelerometers on actual precipitator plate measurements.

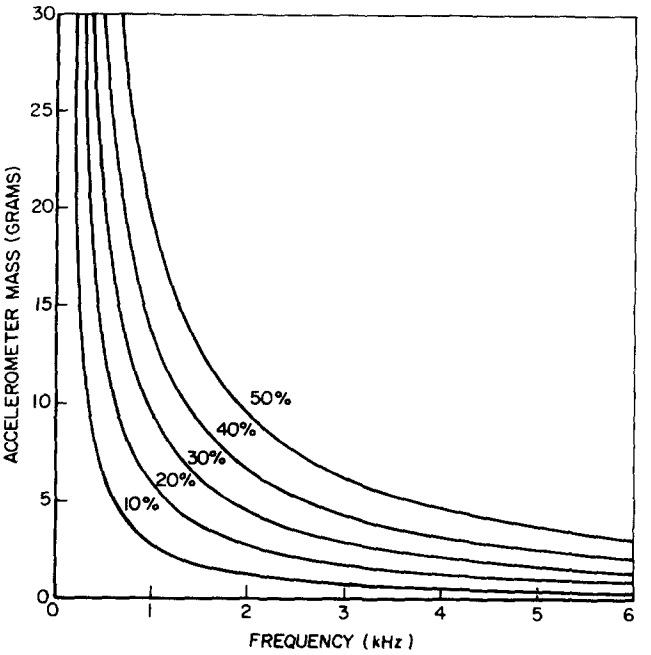

Fig. 7. Acceleration reduction contours 20 gage plate (0.0359 in.).

The concept of the complex frequency response is combined with the Fourier analysis in Section 3, where we demonstrate the use of a numerical filtering method in bringing an experimental result and a corresponding numerical prediction closer together.

Acknowledgement—This work has been carried out under a Grant to Princeton University from the Electric Power Research Institute as part of the program, "Electrostatic Precipitator Plate Rapping and Reliability", which goes together with a parallel research program at Research-Cottrell, Inc. We wish to acknowledge Dr. Owen Tassicker's guidance as program director for EPRI on this research project. We also wish to thank Dr. Tassicker for suggesting the accelerometer problem. We would like to thank Dr. Attila Askar, Visiting Professor in the Department of Civil Engineering, for a very helpful discussion. The computation and drawing of the filtered data have been performed by Mr. William Glennie, Graduate Research Assistant, for which we are very grateful. We further acknowledge the help of Mr. S. Rummel and Mr. F. Jeselsohn of Research-Cottrell and Mr. G. Hieber of Hieber Engineering.

REFERENCES

1. Comments made by O. J. Tassicker at a meeting on the E.P.R.I. Research Program, held at Research-Cottrell, Inc., Bound Brook, New Jersey (2 March 1977).
2. G. Hieber, Plane Plate Rapping Experiment, E.P.R.I. Plate Rapping and Reliability Study, Hieber Engineering Company, Watchung, New Jersey (June 1977) (unpublished).
3. A. W. Leissa, Vibration of Plates, NASA SP-160, Chap. 1, *Sci. Tech. Info. Div.*, NASA, Washington, D.C. (1969).
4. P. M. Morse and K. U. Ingard, *Theoretical Acoustics*, pp. 400–403. McGraw-Hill, New York (1968).
5. S. H. Crandall and W. D. Mark, *Random Vibration in Mechanical Systems*, p. 55. Academic Press, New York (1963).
6. F. B. Hildebrand, *Advanced Calculus for Applications*, pp. 142–155. Prentice-Hall, Englewood Cliffs, New Jersey (1962).
7. Y. H. Pao and C. C. Mow, *Diffraction of Elastic Waves and Dynamic Stress Concentrations*, pp. 326–344. Crane Russak, New York (1973).
8. F. W. J. Olver, Bessel Functions of Integer Order, In *Handbook of Mathematical Functions*, Chap. 9 (Edited by M. Abramowitz and I. A. Stegun). Dover, New York (1968).
9. N. Chang, D. P. Billington and D. A. Nagy, Effects of Acceleration Mass on the Flexural Vibrations of Plates, Dept. of Civil Engng, *Res. Rep.* 77-*SM*-8 (June 1977).
10. A. E. H. Love, *A Treatise on the Mathematical Theory of Elasticity*, 497–498. Dover, New York (1944).
11. J. W. Miles, Motion of a rigid cylinder due to a plane elastic wave. *J. Acoust. Soc. Am.*, **32**, 1656–1659 (1960).
12. D. A. Nagy, N. Chang, D. P. Billington and W. Glennie, Finite Element Numerical Studies of Electrostatic Precipitator Plates. 77-SM-9, Dept. of Civil Engng, Princeton University (1977).